npg

ARTICLE

Craniofacial characteristics of fragile X syndrome in mouse and man

Inge Heulens[1], Michael Suttie[2], Andrei Postnov[3], Nora De Clerck[3], Concetta S Perrotta[3], Teresa Mattina[4], Francesca Faravelli[5], Francesca Forzano[5], R Frank Kooy[1] and Peter Hammond*,[2]

For a disorder as common as fragile X syndrome, the most common hereditary form of cognitive impairment, the facial features are relatively ill defined. An elongated face and prominent ears are the most commonly accepted dysmorphic hallmarks. We analysed 3D facial photographs of 51 males and 15 females with full *FMR1* mutations and 9 females with a premutation using dense-surface modelling techniques and a new technique that forms a directed graph with normalized face shapes as nodes and edges linking those with closest dysmorphism. In addition to reconfirming known features, we confirmed the occurrence of some at an earlier age than previously recorded. We also identified as yet unrecorded facial characteristics such as reduced facial depth, hypoplasticity of the nasal bone–cartilage interface and narrow mid-facial width exaggerating ear prominence. As no consistent craniofacial abnormalities had been reported in animal models, we analysed micro-CT images of the fragile X mouse model. Results indicated altered dimensions in the mandible and both outer and inner skull, with the latter potentially reflecting differences in neuroanatomy. We extrapolated the mouse results to face shape differences of the human fragile X face.

INTRODUCTION

Individuals with fragile X syndrome are characterized by cognitive and behavioural problems. In addition, they exhibit facial characteristics including a long narrow face, prominent ears and a high-arched palate. Other reported facial features are prominence of the jaw, puffiness around the eyes, long palpebral fissures, decreased inner canthal separation, epicanthal folds, strabismus, broad nose and hypotonia.[1,2] The facial features occur in affected males and to a lesser extent in affected females. In practice, it is neither straightforward nor reliable to propose a diagnosis of fragile X syndrome based on facial form alone. Not all of the facial features are recognizable at a young age and most have been recorded only after puberty. This has been particularly true for discriminating facial features such as prominent ears and jaw, and a long face. As for young children, it is not known whether the facial characteristics are absent in youth, or too subtle to notice, and at what age they arise. Observations concerning facial features are based on only a few studies, each describing a relatively small number of affected individuals. For example, reduced face width and increased ear length were first quantified more than two decades ago[3,4] and their relationship with deficit of the *FMR1*-gene product (FMRP) was described more recently.[5]

No consistent craniofacial abnormalities have been reported in animal models of the condition. The fragile X knockout mouse, a validated model for the disorder, showed no visible dysmorphism.[6–8] More recently, anatomical phenotyping in the mouse model using MRI imaging found no significant craniofacial abnormalities.[9] Studies in zebrafish show conflicting results. In the *Fmr1* morpholino-injected zebrafish, defects in the craniofacial pattern were observed.[10] However, in the *Fmr1* knockout zebrafish model no abnormalities were detected.[11] A single study in *Xenopus laevis* reported reduced and deformed cranial cartilage structures in the head after morpholino-knockdown of *Fmr1*.[12]

To analyse craniofacial dysmorphism in fragile X in man and mouse, we captured 3D facial photographs of a large cohort of affected individuals and, in addition, acquired micro-CT images of the heads of knockout mice. In the human study, we also included a small set of premutation carriers, as data were unavailable on the effect of premutation sized repeats on craniofacial development. We employed dense-surface model (DSM) analysis[13,14] and novel signature graph[15] techniques to both human and animal data to confirm known and detect previously unidentified features.

SUBJECTS AND METHODS

Our recruitment of 75 individuals with confirmed pre- or full mutations was through medical genetics clinics in Catania ($n = 10$) and Genova ($n = 24$) in Italy or family support groups in the UK ($n = 32$) and USA ($n = 9$). Table 1 contains a detailed breakdown of gender and age. In addition, 373 images of unrelated healthy controls (185 female; 188 male) were obtained from an existing collection. All individuals reported are of white European origin.

Study mice were housed in standard conditions before killing at 10–12-weeks-old. Skulls and mandibles of 14 wild-type mice and 15 *Fmr1* knockout littermates (C57Bl/6J background) were isolated, and after removing the skin and subcutaneous tissue they were fixed in 70% EtOH for 2 days and remaining skin carefully peeled off to retain skull–mandible connexion. Skulls

[1]Department of Medical Genetics, University of Antwerp, Antwerp, Belgium; [2]Molecular Medicine Unit, UCL Institute of Child Health, London, UK; [3]Department of Biomedical Sciences, University of Antwerp, Antwerp, Belgium; [4]Department of Pediatrics, University of Catania, Catania, Italy; [5]Medical Genetics Unit, Galleria Hospital, Genova, Italy
*Correspondence: Professor P Hammond, Molecular Medicine Unit, UCL Institute of Child Health, 30 Guilford Street, London WC1 1EN, UK. Tel: +44 (0)20 7905 2399; E-mail: p.hammond@ucl.ac.uk

Table 1 Mean age and age ranges of individuals with full mutations and premutations

	Full mutation	Premutation	Total
Male			
N	51	—	51
Mean age (years)	15.7	—	
Age range (years)	2.2–40.8	—	
Female			
N	15	9	24
Mean age (years)	19.5	35.8	
Age range (years)	3.0–45.0	19.6–51.6	
Total			
N	66	9	75

were rehydrated and placed in 1% potassium hydroxide (KOH) refreshed daily for 2 days (or as long as needed) to dissolve the brain. When the skull was completely clean it was stored in glycerol ready for scanning.

All human subjects were recruited under ethical approval with written, informed consent of the individuals concerned or parents or legal guardians. All animal experiments complied with European Community Council Directive (86/609/EEC) and were approved by the Animal Ethics Committee of the University of Antwerp.

Methods

Image preparation for human subjects. Facial images were acquired using commercial 3D photogrammetric cameras and annotated manually by one individual (PH) at 24 anatomical locations: left and right endocanthion, exocanthion, palpebrale superius, palpebrale inferius, preaurale, otobasion inferius, crista philtrum, cheilion and alare; nasion, pronasale, subnasale, labiale superius, labiale inferius and gnathion. (Supplementary Figure 2) These landmarks were previously validated for reproducibility and accuracy.[16] The landmarking and subsequent DSM building were undertaken using software developed in-house.[13,14] The term 'dense surface model' refers to the set of principal components (PCs) or principal components analysis modes accounting for the shape variation in the surfaces. The DSM analysis of the human subjects involved about 28 000 surface points. More details about the construction of DSMs are provided as supplementary information.

Image preparation for animal subjects. Virtual cross-sections of the mice skulls were obtained by X-ray microtomography at a resolution of 20 μm using a desktop micro-CT scanner (Skyscan 1072, Kontich, Belgium). The micro-CT volumes were uniformly down-sampled with respect to three orthogonal axes, reducing voxel density by a factor of 8, to provide a more manageable number of 3D points on the segmented surfaces. The MIMICS and microView software tools were used to segment skull and mandible components in a semi-automated fashion. Segmented surfaces were manually landmarked by one individual (pH). In all, 120 landmarks were used on skull, mandible and inner skull as illustrated in Supplementary Figure 1. Because of the re-entrant nature of the skull surface, we limited the DSM building to regions shown in Figure 5. Approximately 460 000 surface points across the skull of each mouse were employed in DSM analysis as with the human faces.

Face signature. Face signature is normalized face shape with respect to age and sex-matched controls. Heat maps of tens of thousands of face surface points are used to visualize variation in position difference in a face signature from the mean of matched controls at a chosen statistical significance. The differences can be orthogonal to the face surface or parallel to the usual transverse, vertical and anterior–posterior axes. The distance between two face signatures is the Euclidean distance between vectors representing their heat maps. In a face signature graph, an edge is drawn from one face signature to another if the second is closest to the first. Signature graphs have been successfully used recently to link extreme facial dysmorphism in patients with

epilepsy to novel micro-deletions and duplications[17,18] and rare conditions such as fibrodysplasia ossificans progressiva.[19] Face–brain shape correlation studies in mouse models have also benefitted from signature graph techniques.[20] Further technical details are provided as supplementary information and elsewhere.[15] All signature graphs were drawn using the Graphviz software.[21]

RESULTS

Comparison of average faces of males with a full mutation and healthy controls confirms known and suggests new facial characteristics

An animated morph between the average face of 50 males with a full mutation and that of 50 contiguously aged male controls with a matching mean age is available as FULL_MUTATION_MORPH.AVI in the supplementary information. This animation highlights known fragile X facial features such as the long and narrow face, broad nose and hypotonia–the latter demonstrated by slackness of the lower jaw. Ear prominence is not immediately obvious in the portrait view, but on closer scrutiny greater exposure of the ear surface does occur, although more by narrowing of the face proximal to the temporomandibular joint (TMJ). Both portrait and profile views suggest a more open periorbit, broader philtrum (portrait), reduced facial depth (profile) and flatness across the nasal bridge (profile).

These differences are colour-coded on a scale of ±1 SD of significance in heat-map comparisons of the same average faces (Figure 1c–e) in terms of displacement of densely corresponded points parallel to the usual three orthogonal axes. Figure 1c documents the wider nose and philtrum (at 1 SD), the narrowness (at about 0.5 SD) close to the TMJ and the previously undocumented narrowing (at 1 SD) at the nasal bone–cartilage interface. Figure 1d records the taller orbit and upward displacement of the nasal alae and proximal mid-face (blue colouring), as well as the hypotonic droop of the lower lip and chin (red/yellow). Figure 1e reflects the reduced facial depth and flattening of the nasal bridge. These visualized differences are assessed quantitatively below using appropriate measures.

Face length and growth in fragile X syndrome

We compared the face length (nasion to gnathion) of individuals with fragile X syndrome and premutation carriers to that of controls using the two age groups: juvenile (≤ 20 years) and adult (> 20 years). Face length (Figure 2a) was significantly greater in full mutation juvenile males ($P < 0.001$) and full mutation adult males ($P < 0.0001$) compared with age-matched controls. Females with a full mutation also had significantly long faces compared with controls ($P < 0.001$), but premutation cases did not (Figure 2b). Besides face length, we analysed facial growth, which is captured in the first PC (PC1) of a DSM. PC1 is highly correlated with age (Figure 2c and d). For individuals with a full mutation, facial growth is greater than controls from an early age and remains consistently so over time (juvenile males: $P < 0.001$; juvenile females: $P < 0.001$; adult males: $P = 0.02$). A face growth comparison for premutation females did not reach significance.

Vertical face shape in fragile X syndrome

The second PC, PC2, typically reflects face shape variation from long and narrow to short and square, as can be seen from the face annotations of the ordinate axis of Figure 2e. Compared with controls, most full mutation males score below average for PC2 and once again from an early age (juveniles: $P < 0.001$; adults: $P = 0.04$).

This was echoed in PC2 for full mutation females ($P = 0.014$), but not for premutation cases (Figure 2f).

Face signatures for vertical difference for 67-affected individuals (Figure 3a–c) delineate degrees of face lengthening in heat maps at a
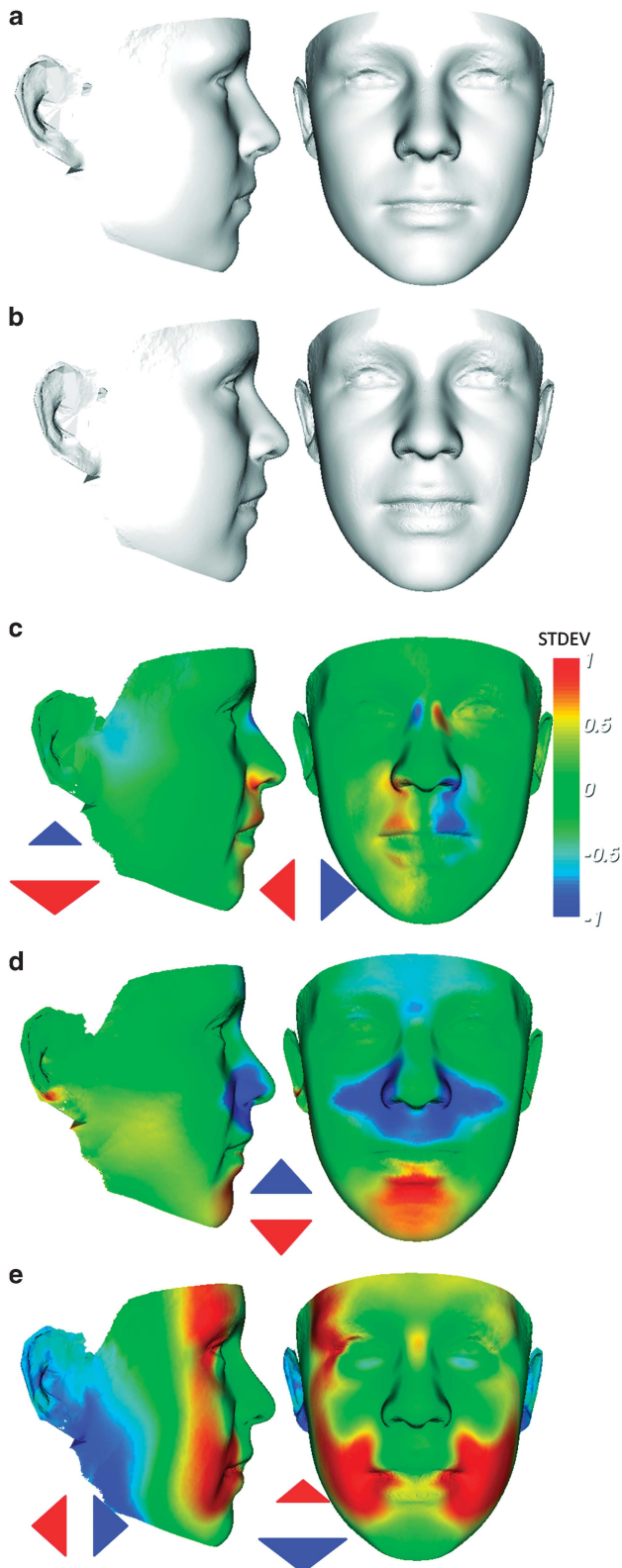
significance of 3 SD (red/blue reflects upward/downward displacement). Once again, significant difference is evident in full mutation males (Figure 3a), less so in full mutation females (Figure 3b) and not at all in premutation cases (Figure 3c). Only a handful of face signatures of 304 controls showed similar vertical facial difference at 3 SD (data not shown).

The face signature graph for normalized vertical difference for 47 males with a full mutation has eight subclusters (Figure 3d). For lack of matching controls, some younger full mutation males had to be omitted from signature graph analyses. Generally speaking, face signatures segregating to the lower half of this graph have less vertical lengthening of the face. Notice that clusters 3 and 5 identify four individuals (individually framed in Figure 3a) whose obvious grin distorts their face shape. Cluster 8 contains males with a full mutation with the most extreme vertical face difference.

The signature graph for vertical face difference for all 47 males with a full mutation and 150 male controls is shown in Figure 4a. The vertices of the graph representing full mutation cases (black filled) are almost all leaf nodes or sequences, with some clusters from Figure 3d retaining connectivity in Figure 4a. For example, cluster 8 of Figure 3d becomes cluster 8 and part of cluster 10 in Figure 4a. This retention of signature connectivity, even when controls are introduced, reflects greater affinity of some fragile X individuals in terms of vertical face shape difference. This is echoed in a low dispersion index, 0.09, for controls (Figure 4b). On the other hand, the higher dispersion index of 0.76 for full mutation males, reflecting a few superclusters and many singletons, indicates heterogeneity in vertical face shape difference when they are considered as a whole. This concurs with visual inspection of individual signatures (Figure 3a).

Face depth in full mutation males

Face depth at the eye–ear level was estimated as the distance between the mid-inner canthal and mid-preaurale points. Compared with controls, adult full mutation males have a significantly shallower mean face depth ($P = 0.036$). For juveniles with a full mutation, this measure of face depth (Figure 2h) starts out significantly larger ($P = 0.022$) and increases at a rate slower than matched male controls, but not with statistical significance ($P = 0.070$). A similar depth measure using mid-outer canthal and mid-preaurale points achieves significance for all males with a full mutation, largely due to a significant reduction in the relative inclination of the palpebral fissures (juvenile male with full mutation: $P = 0.04$; adult male with full mutation: $P < 0.01$) as measured by the angle between the lines linking inner and outer canthi of each eye.

Ear prominence in fragile X syndrome

The much quoted prominence of ears in fragile X syndrome was reconfirmed in this study. However, the narrowness of the faces of

Figure 1 Average faces of 50 full mutation male individuals with fragile X syndrome (**b**) and 50 healthy controls (**a**) with same mean age. Heat maps of position difference with respect to three orthogonal axes for densely corresponded points on surface of average of individuals with a full mutation compared with corresponding position on average of 50-matched male controls. The lateral axis comparison (**c**) highlights narrow nasal bridge, broader nose and philtrum, narrowness at TMJ and hypotelorism; the vertical comparison (**d**) reflects upward displacement of the supraorbit and hypotonic droop of the lower jaw; the anterior–posterior comparison (**e**) shows flattening at the nasal bridge, posterior displacement of the outer canthi and reduced facial depth. The red–green–blue range reflects displacement parallel to the axis concerned with maximal red–blue at 1 SD in opposing directions and green at 0 SD.
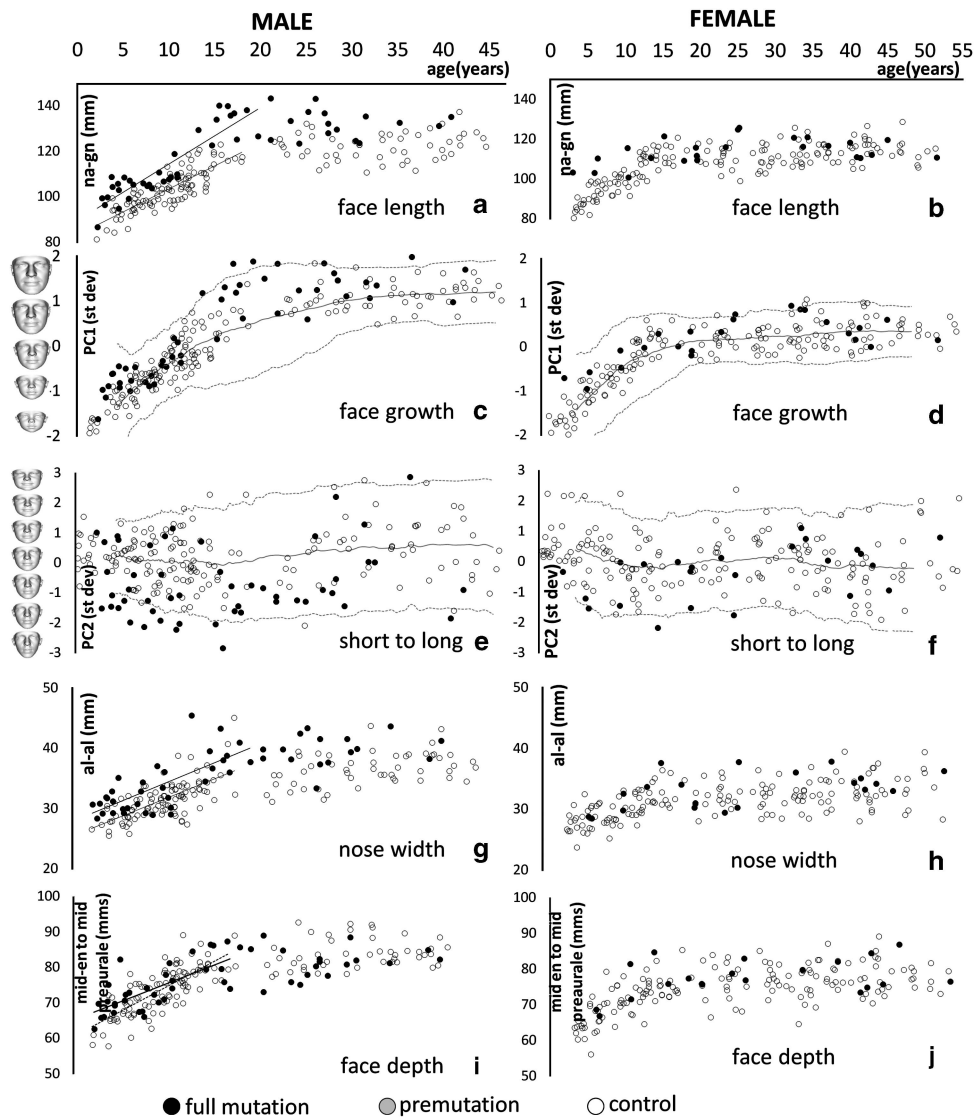
Figure 2 Male and female scatterplots of age against different face dimensions of individuals with fragile X syndrome and controls. Face length was measured as distance between *nasion* and *gnathion* (a–b). Face growth was captured by the principal components analysis mode PC1 (c–d), and long and narrow to short and square-face shape variation was delineated by PC2 (e–f). The ordinate axis is annotated with warps of the mean face of both affected and control individuals at particular values of PC1/PC2. Nose width is distance between nasal alae (g–h). Face depth measured at eye level (mid-en to mid-preaurale) is shown in (i–j).

some affected males exaggerated their ear prominence. This is best shown by animations between the faces of affected males and age–sex-matched mean faces used to compute signatures. Supplementary animation *Outer_Face_Animations.avi* clearly shows that in some cases an individual's ears are no more prominent than those of the matched control mean. It is the narrowness of their mid-face that exaggerates ear prominence. Interestingly, if the central part of the face is omitted and only the outer face, as in the morphs, is used as the basis for face shape discrimination testing between control and full mutation males, a score of 0.96 is achieved (see later section for details). This provides further confirmation of considerable shape differences from controls in terms of round-oval face spectrum and ear shape.

### The nasal phenotype of fragile X syndrome
For individuals with a full mutation, nasal width, distance between nasal alae, (Figure 2g and h) was significantly greater than in male

controls (juveniles: $P < 0.001$; adults: $P < 0.001$). The nasal width of females with either a full or premutation was not significantly different from controls. For half of the full mutation males, normalized nose shape shows localized deficiency of 3 SD at the nasal bone (Figure 3e). Less than 10% of control male noses show similar deficiency and even then well below 3 SD (data not shown).

Discrimination between faces of full mutation males and controls
Having identified face shape differences in affected individuals, we determined their ability to discriminate between the faces of males with FRAGILE X syndrome and those of male controls. We used multi-folded cross validation of 20 randomly generated and stratified training-unseen test set pairs. The discrimination rate is expressed in terms of mean area under 20 ROC (receiver operating characteristic) curves and corresponds to the probability of correctly classifying a pair of randomly selected faces, one from each of the affected and
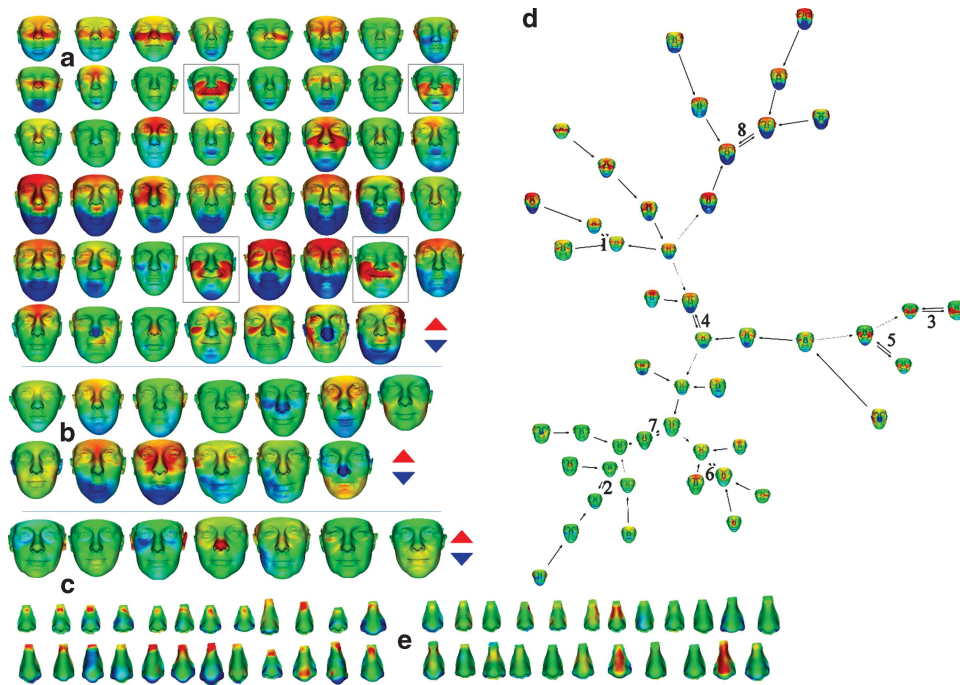
Figure 3 Face signatures for vertical shape difference for individuals with fragile X syndrome: (**a**) males with full mutation ($n = 47$); (**b**) females with full mutation ($n = 13$); (**c**) females with premutation ($n = 7$). Deep red/blue indicates regions displaced ≥ 3 SD upwards/downwards relative to matched mean; (**d**) face signature graph for vertical difference for males with full mutation; (**e**) 24 of 47 nose signatures at 3 SD (shown to left of '**e**' label) showing localized deficiencies on or close to the nasal bone/nasal cartilage interface with a simultaneous broadening at the nasal tip. Blue/red indicates relative expansion/contraction relative to the mean-matched control.
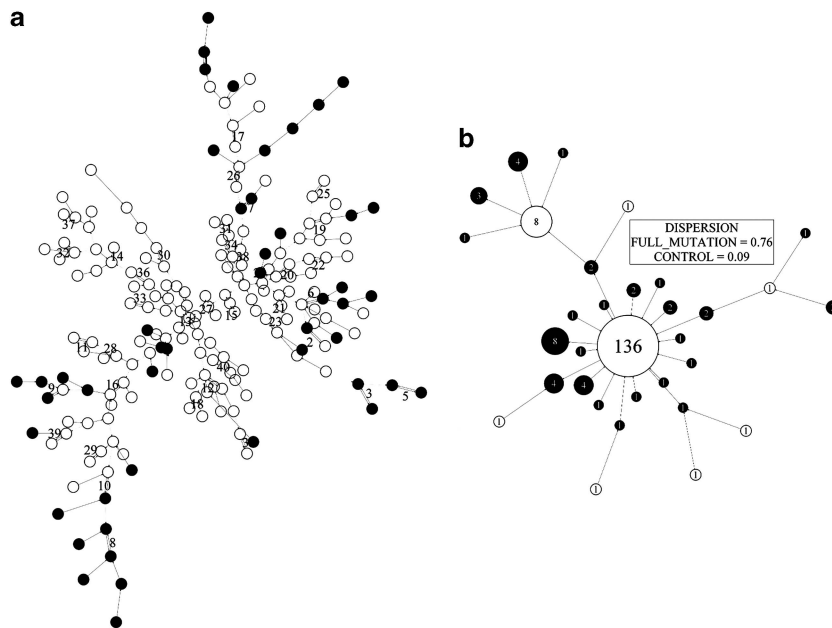
Figure 4 Face signature graph for normalized vertical difference for 47 males with a full mutation and 150 male controls: (**a**) binary form: control (blank); full mutation (black); (**b**) collapsed form: control (blank); full mutation (black); emphasizing outlier status of most full mutation males.

unaffected cohorts. Optimal discrimination results for four surface patches *face with ears/face without ears/outer face with ears/nose*, calculated with three different pattern recognition algorithms are as follows: closest mean (0.96/0.96/0.96/0.93); linear discriminant analysis (0.99/0.98/0.98/0.97) and support vector machines (0.99/0.97/0.98/0.97). For linear discriminant analysis, the goal is a linear combination of PC modes that exhibits the largest difference in the subgroup means relative to the within-group variance. Support vector

machines, or large margin classifiers, focus on individuals in the overlap of subgroups that determine a surface with largest separating margin.

Fmr1 KO mice display significant mandible and skull differences

Separate DSMs for mandible and skull patches identified localized regions of axial differences in KO means normalized against wild-type. Figure 5A–E reveal several shape differences: parietal bone lengthening (a); inter-parietal bone shortening (b); widening of premaxilla and narrowing of posterior parietal bone (**B**); a depression at the centre of the skull vault (c); differences at the coronoid process tips and angle of the mandible (**D**); and transverse mandibular narrowing at the level of the articular surfaces (f).

Once the surface comparison had identified regions of difference, landmark-based anatomical measurements were used where possible to establish statistical significance: shorter inter-parietal bone ($P = 0.001$); reduced skull vault height at junction of parietal and inter-parietal bones ($P = 0.003$); reduced width of mandible at articular surface of the tempero-mandibular joint ($P = 0.028$); and greater angle subtended at the anterior articular surface from tips of the coronoid process and angle of the mandible ($P = 0.035$). These

and other differences not quite reaching statistical significance are documented in Table 2. The results for the skull and mandible are also visualized in dynamic morphs between corresponding averages of KO and wild-type groups (see supplementary videos SKULL_ANIMA-TION.avi and MANDIBLE_ANIMATION.avi).

The reduced inter-parietal bone length in combination with diminished height at juncture with the parietal bone might have implications for the underlying brain shape. More specifically, the latter suggests possible differences in the region of the cerebellum. Therefore, besides the outer skull, we also analysed the inner skull as a surrogate for brain shape. Both length (Figure 5g; $P = 0.033$) and rear width (Figure 5h; $P = 0.015$) of the inner skull are significantly decreased in KO mice.

A separate DSM was generated for a patch of the maxilla corresponding to the nasal bone. Figure 5G shows the nasal bone signatures and Figure 5H the resulting signature graph for differences along the surface normal. This analysis shows swelling at the outer edge of the nasal bone (4G) and an almost perfect partition of KO (black framed) and control mice (frameless) nodes in the signature graph (5H).

Craniofacial anomalies in fragile X syndrome and fmr1 KO mice

Extrapolation of the results of the KO mice to the craniofacial anomalies of affected individuals shows some resemblance. Although a long face and tall forehead are characteristics of fragile X syndrome, no difference in the anterior–posterior length of the skull and the length of the frontal bone was found in the *fmr1* KO mouse. However, increased height of the mandible body and enlarged angle between the coronoid, condylar and angular processes combine to increase vertical dimensions of the mandible-skull complex. The reduced lateral separation of the condylar surfaces, the narrower parietal bone width and posterior width of the inner skull in the knockout mice result in a narrower mandible and skull near the tempero-mandibular joint. This could correspond to the more oval facial form found in fragile X individuals and the mid-facial narrowing that accentuates ear prominence in some affected males. The increased width of the premaxilla (Figure 5B) and nasal bone differences (Figure 5C and Figure 5G and H) have their counterparts in the wider nose and shape differences found in affected individuals at the nasal bone–cartilage interface.

DISCUSSION

The facial characteristics of fragile X syndrome, and of developmental disorders in common, are often very subtle. In order to help diagnose this condition and related genetic disorders, various pattern recognition techniques have been used to detect related facial dysmorphism. An early study employed thirty anthropometric facial and somatic measurements along with discriminant analysis to establish detection rates of 95% in full mutation males and 85% in full mutation females.[3] As the authors point out, these rates may be overestimated by 5% or so because the testing was not blinded. Classification based on 2D images of face shape alone achieved a recognition rate for fragile X syndrome between 75 and 99.9%, depending on the technique used.[22,23] The overall syndrome recognition rate of 10 different syndromes ranged between 52 and 76%, confirming that computer-based methods are able to recognize some syndrome-related facial characteristics better than others. Studies using DSMs of 3D face shape have delineated common facial features in a range of neurodevelopmental conditions, often, in addition, establishing accurate discriminating characteristics or assisting the determination of phenotype–genotype correlations.[24–27]
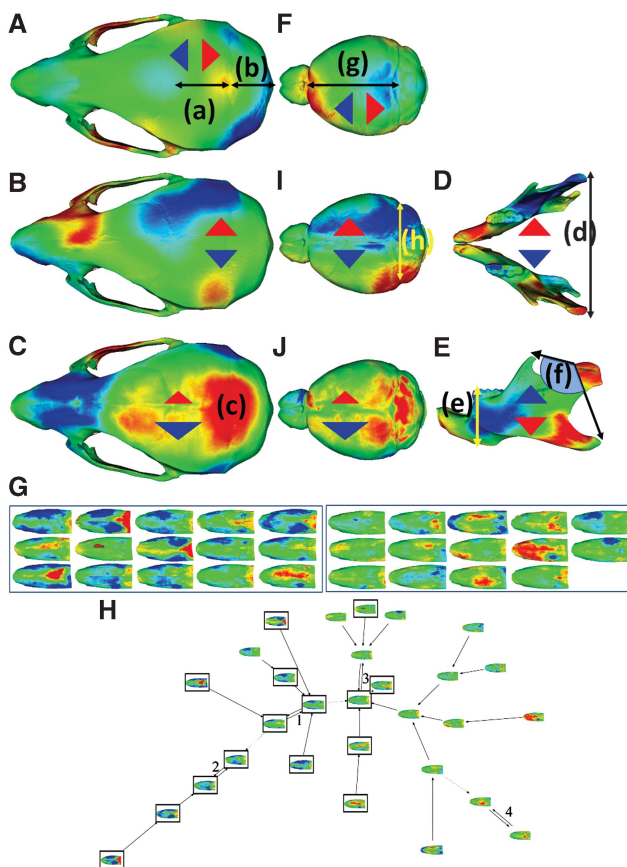
Figure 5 Shape differences in the mean knockout-mouse skull heat mapped at 1 SD compared with the mean wild-type mouse skull along three orthogonal axes: anterior–posterior (**A**), lateral (**B**) and dorsal–ventral (**C**). Similar comparisons were made for the mandible, vertically (**D**) and laterally (**E**), and the inner skull, two axes (**F**), again heat mapped at 1 SD nasal bone signatures for difference along surface normal for knockout and wild-type mice at 1 SD (**G**) and associated signature graph showing marked separation in the clustering reflecting the shape difference (**H**) between WT (frameless) and KO (framed).

Table 2 Comparison of anatomical measures for wild-type and knockout mice

| | Parietal | Inter-parietal | Skull vault | Mandible | | | Inner skull | |
	Length (a)	Length (b)	Height (c)	Angle (d)	Depth (e)	Width (f)	Length (g)	Width (h)
Mean								
Fmr⁻˒⁻ (N = 15)	106.2	92.7	112.9	127.6	211.8	548.5	216.9	218.4
WT (N = 14)	101.3	98.5	119.0	120.8	208.3	558.5	219.8	223.4
P-value	0.078	0.001**	0.003**	0.035*	0.073	0.028*	0.033*	0.015*

Abbreviation: WT, wild-type. (a) to (h) refer to the measurements defined in Figure 5.
*Significance at $P \leqslant 0.05$.
**Significance at $P \leqslant 0.005$.

In this study, we compared the faces of 66 individuals with fragile X syndrome with those of several hundred unrelated controls. Depending on the pattern recognition technique used and the face surface patch studied, we established discrimination rates between 96 and 99%. Previously, results concerning bizygomatic and bigonial narrowing, especially in full mutation males, were first quantified in adults[3] and later in children as young as 4 years.[4,5] We identified as yet unrecorded facial characteristics such as hypoplasticity of the nasal bone–cartilage interface and ear prominence exaggerated by narrowing of the mid-face. The most classical facial features of the fragile X syndrome, such as the long, narrow face and protruding ears, could also be confirmed in our study. In addition, it was clear that the long face begins at an earlier age than previously thought and becomes more pronounced with age. One remark has to be made concerning the prominence of the ears. This is one of the most reported hallmarks of fragile X syndrome, but it now seems the apparent ear prominence is often a consequence of the extremely narrow mid-face.

We also performed an extensive craniofacial assessment of the *Fmr1* KO mouse. Reduced inter-parietal bone length, reduced skull vault height and reduced length and width of the inner skull and some abnormalities in the mandible were observed in the fragile X mouse[6] compared with wild-type mice. Recently, Ellegood et al[9] also analysed fragile X mouse skulls. However, they did not detect any statistically significant craniofacial anomalies. One possible explanation is the way in which the images were analysed. Where Ellegood et al, used only landmarked-based distances to look for differences, we used DSMs to identify where the differences are and when possible confirmed them with linear or angular measurements.

We also introduced a new technique where we can colour map not just differences in position in terms of mms or microns but also in SDs relative to reference populations of human controls or wild-type mice. This approach delineates the most significant differences in a regional fashion and is particularly useful for surface shape differences where landmarks cannot even be placed. Finally, the number and age of mice used in both the studies varies. We used 14 wild-type mice and 15 knockout mice that were 10–12 weeks of age, while Ellegood et al, used only seven mice per genotype that were 1-month old. Small skeletal differences might not be detected due to smaller numbers in each group or the younger age as we see in humans where some facial characteristics are not obvious in childhood.

The observed skeletal malformations might have consequences for brain volume. Several MRI studies have been performed in individuals with fragile X syndrome, as well as in fragile X mice. In human brains, most findings are related to small deviations such as abnormalities in the hippocampus,[28] the amygdala[29] and the ventricular system.[30] Gross volumetric changes were found in the underdevelopment of the cerebellar vermis.[31] Early studies in the fragile X mouse found no brain volume changes.[32] However, another study showed significant volume decrease of the arbour vita of the cerebellum and more specifically of the deep cerebellar nuclei. Trends were found in the striatum (decrease) and the cerebral cortex of the parieto-temporal lobe (increase).[8] Differences found in the cerebellum are most prominent both in fragile X patients and fragile X mice. The decreased width of the inner skull of fragile X mice seems to correlate with these findings.

Some of the craniofacial differences, for example, human nasal cartilage deficiency and mid-facial effects in the mouse model, correspond in both species and suggest a common mechanism. This supports reports that *FMR1*, the gene silenced in the disorder, influences eye and cranial cartilage development through effects on neural crest cells. This is consistent with a previous study of Bardet-Biedl syndrome where similar nasal bone and mid-facial abnormalities were linked to adverse neural crest cell behaviour.[33] Cranial neural crest cells (CNCC) are pluripotent, mesenchymal cells that arise at the junction between the neural plate and the surface ectoderm, and they are involved in the formation of the craniofacial skeleton.[34] They are also implicated in the formation of nerves, ganglia, cartilage, bone and connective tissue. CNCC migrate in three different streams into the pharyngeal arches, which are a part of the growing embryo that is responsible for the formation of the future head and neck region. As a consequence, craniofacial malformations can be caused by defects in the proliferation, migration or differentiation of CNCC. Some of the key players in these processes are the Homeobox transcription factor (*Hox*) genes, Sonic Hedgehog and Wnt signalling. The reduction of FMRP dysregulates Wnt function and so adversely affects cell migration. In fragile X syndrome, a few links between *Fmr1* and the neural crest have been described. In *Fmr1* morpholino-injected zebrafish, a reduction of *dlx-2a*, a Hox gene, was found, indicating that loss of *Fmr1* has an effect on neural cell crest specification.[10] This resulted in defects in the craniofacial pattern, more specific in the angle and width of Meckles' cartilage. Downregulation of *Fmr1* in *Fmr1* morpholino-injected *X. laevis*, resulted in a severe migration defect of neural crest cells, with reduced and deformed cranial cartilage structures as a consequence.[12] Involvement of the miRNA pathway in this process was proposed. However, in the *Fmr1* knockout zebrafish, no craniofacial malformations could be detected.[11]

In conclusion, we have refined the facial characteristics of fragile X syndrome and demonstrated high rates of discrimination between the facial features of affected and control males. We were able to reconfirm several known craniofacial abnormalities and report new anomalies in fragile X syndrome. These findings could be helpful for clinical geneticists in diagnosis. In addition, we observed the same malformations in the fragile X knockout mouse model, reinforcing it

as the best validated animal model to study fragile X syndrome, not only for behavioural, molecular or electrophysiological studies but also for studies concerning developmental biology. Further investigation is required to unravel the role of FMRP in the formation of the craniofacial skeleton.

CONFLICT OF INTEREST

The authors declare no conflict of interest.

1 Hagerman RJ: Physical and behavioral phenotype; In Hagerman RJ, Hagerman. PJ (eds) *Fragile X syndrome: diagnosis, treatment and research*. Johns Hopkins University Press: Baltimore, MA, 2002.
2 Butler MG, Allen GA, Singh DN, Carpenter NJ, Hall BD: Photoanthropometric analysis of individuals with the fragile X syndrome. *Am J Med Gen* 1988; **30**: 165–168.
3 Loesch DZ, Lafranchi M, Scott D: Anthropometry in martin-bell syndrome. *Am J Med Gen* 1988; **30**: 149–164.
4 Loesch DZ, Sampson ML: Effects of the fragile X anomaly on body proportions estimated by pedigree analysis. *Clin Genet* 1993; **44**: 82–88.
5 Loesch DZ, Huggins RM, Bui QM, Taylor AK, Hagerman RJ: Relationship of deficits of FMR1 gene specific protein with physical phenotype of fragile X males and females in pedigrees: a new perspective. *Am J Med Gen* 2003; **118A**: 127–134.
6 Bakker CE, Verheij C, Willemsen R *et al*: Fmr1 knockout mice: a model to study fragile X mental retardation. *Cell* 1994; **78**: 23–33.
7 Bakker CE, Oostra BA: Understanding fragile X syndrome: insights from animal models. *Cytogenet Genome Res* 2002; **100**: 111–123.
8 Kooy RF: Of mice and the fragile X syndrome. *Trends Genet* 2003; **19**: 148–154.
9 Ellegood J, Pacey LK, Hampson DR, Lerch JP, Henkelman RM: Anatomical phenotyping in a mouse model of fragile X syndrome with magnetic resonance imaging. *Neuroimage* 2010; **53**: 1023–1029.
10 Tucker B, Richards RI, Lardelli M: Contribution of mGluR and Fmr1 functional pathways to neurite morphogenesis, craniofacial development and fragile X syndrome. *Hum Mol Genet* 2006; **15**: 3446–3458.
11 den Broeder MJ, van der Linde J, Brouwer JR *et al*: Generation and characterization of FMR1 knockout zebrafish. *PLoS One* 2009; **4**: e7910.
12 Gessert S, Bugner V, Tecza A, Pinker M, Kuhl M: FMR1/FXR1 and the miRNA pathway are required for eye and neural crest development. *Dev Biol* 2010; **341**: 222–235.
13 Hutton TJ, Buxton BF, Hammond P, Potts HW: Estimating average growth trajectories in shape-space using kernel smoothing. *IEEE Trans Med Imaging* 2003; **22**: 747–753.
14 Hammond P: The use of 3D face shape modelling in dysmorphology. *Arch Dis Child* 2007; **92**: 1120–1126.
15 Hammond P, Suttie M: Large scale objective phenotyping of facial morphology in 3D. *Hum Mut* 2012; **33**: 817–825.
16 Gwilliam JR, Cunningham SJ, Hutton TJ: Reproducibility of soft tissue landmarks on three-dimensional facial scans. *Eur J Orthod* 2006; **28**: 5.
17 Novy J, Catarino CB, Chinthapalli k *et al*: Vaccine encephalopathy is not exclusively Dravet syndrome: a case of Angelman syndrome. *Eur J Med Genet* 2012; **55**: 338–341.
18 Chinthapalli K, Bartolin E, Novy J *et al*: Atypical face shape and genomic structural variants in epilepsy. *Brain* 2012; **135**: 3101–3114.
19 Hammond P, Suttie M, Hennekam RC *et al*: The facial signature of fibrodysplasia ossificans progressiva. *Am J Med Genet* 2012; **158A**: 1368–1380.
20 Lipinski RJ, Hammond P, O'Leary-Moore SK *et al*: Stage-specific ethanol exposure causes unique face-brain dysmorphology patterns in a mouse model of fetal alcohol spectrum disorder. *PLOS ONE* 2012; **7**: e43067.
21 Ellson J, Gansber E, Koutsofios L, North S, Woodhull G: Graphviz—Open source graph drawing tools. *Lect Notes Comput Sci* 2002; **2265**: 594–597.
22 Loos H, Wieczorek D, Wurtz RP, von der Malsburg C, Horsthemke B: Computer-based recognition of dysmorphic faces. *Eur J Hum Genet* 2003; **11**: 555–560.
23 Boehringer S, Vollmar T, Tasse C *et al*: Syndrome identification based on 2D analysis software. *Eur J Hum Genet* 2006; **14**: 1082–1089.
24 Bhuiyan ZA, Klein M, Hammond P *et al*: Genotype-phenotype correlations of 39 patients with Cornelia De Lange syndrome: the Dutch experience. *J Med Genet* 2006; **43**: 568–575.
25 Hammond P, Hutton TJ, Allanson JE *et al*: Discriminating power of localized three-dimensional facial morphology. *Am J Hum Genet* 2005; **77**: 999–1010.
26 Dalal AB, Phadke SR: Morphometric analysis of face in dysmorphology. *Comput Methods Programs Biomed* 2007; **85**: 165–172.
27 Hammond P, Hannes F, Suttie M *et al*: Fine grained facial phenotyping in Wolf-Hirschhorn Syndrome. *Eur J Hum Genet* 2012; **20**: 33–40.
28 Reiss AL, Abrams MT, Greenlaw R, Freund L, Denckla MB: Neurodevelopmental effects of the FMR1 full mutation in humans. *Nat Med* 1995; **1**: 159–167.
29 Mostofsky SH, Mazzocco MMM, Aakalu G *et al*: Decreased cerebellar posterior vermis size in fragile X syndrome. Correlation with neurocognitive performance. *Neurology* 1998; **50**: 121–130.
30 Reiss AL, Aylward E, Freund LS, Joshi PJ, Bryan RN: Neuroanatomy of fragile X syndrome: the posterior fossa. *Ann Neurol* 1991; **29**: 26–32.
31 Reiss AL, Patel S, Kumar AJ, Freund L: Neuroanatomical variations of the posterior fossa in men with the fragile X (Martin-Bell) syndrome. *Am J Med Genet* 1988; **31**: 407–414.
32 Kooy RF, Reyniers E, Verhoye M *et al*: Neuroanatomy of the fragile X knockout mouse brain studied using in *vivo* high resolution magnetic resonance imaging. *Eur J Hum Genet* 1999; **7**: 526–532.
33 Tobin JL, Di Franco M, Eichers E *et al*: Inhibition of neural crest migration underlies craniofacial dysmorphology and Hirschsprung's disease in Bardet-Biedl syndrome. *Proc Natl Acad Sci USA* 2008; **105**: 6714–6719.
34 Trainor PA, Krumlauf R: Hox genes, neural crest cells and branchial arch patterning. *Curr Opin Cell Biol* 2001; **13**: 698–705.

Supplementary Information accompanies the paper on European Journal of Human Genetics website (http://www.nature.com/ejhg)